



UNIVERSITY OF LEEDS

This is a repository copy of *High-Mobility Toolkit for Quantum Dot Films*.

White Rose Research Online URL for this paper:

<http://eprints.whiterose.ac.uk/107605/>

Version: Accepted Version

Article:

Gómez-Campos, FM, Rodríguez-Bolívar, S and Califano, M (2016) High-Mobility Toolkit for Quantum Dot Films. *ACS Photonics*, 3 (11). pp. 2059-2067. ISSN 2330-4022

<https://doi.org/10.1021/acsp Photonics.6b00377>

Reuse

Unless indicated otherwise, fulltext items are protected by copyright with all rights reserved. The copyright exception in section 29 of the Copyright, Designs and Patents Act 1988 allows the making of a single copy solely for the purpose of non-commercial research or private study within the limits of fair dealing. The publisher or other rights-holder may allow further reproduction and re-use of this version - refer to the White Rose Research Online record for this item. Where records identify the publisher as the copyright holder, users can verify any specific terms of use on the publisher's website.

Takedown

If you consider content in White Rose Research Online to be in breach of UK law, please notify us by emailing eprints@whiterose.ac.uk including the URL of the record and the reason for the withdrawal request.



eprints@whiterose.ac.uk
<https://eprints.whiterose.ac.uk/>

High-mobility toolkit for quantum dot films

Francisco M. Gómez-Campos,^{†,‡} Salvador Rodríguez-Bolívar,^{†,‡} and Marco
Califano ^{*,¶}

*Departamento de Electrónica y Tecnología de Computadores, Facultad de Ciencias, Universidad
de Granada, 18071 Granada, Spain , CITIC-UGR, C/ Periodista Rafael Gómez Montero, n 2,
Granada, Spain , and Institute of Microwaves and Photonics, School of Electronic and Electrical
Engineering, University of Leeds, Leeds LS2 9JT, United Kingdom*

E-mail: m.califano@leeds.ac.uk

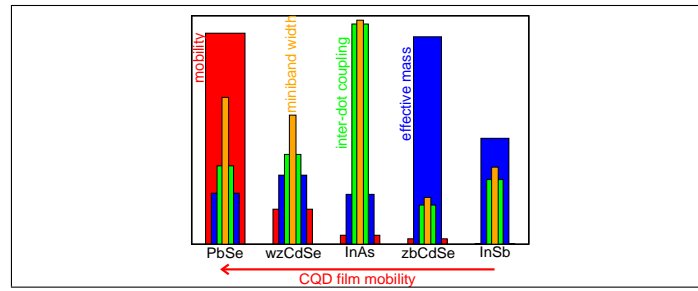
*To whom correspondence should be addressed

[†]Granada

[‡]CITIC-UGR

[¶]Leeds

Graphical TOC Entry



Abstract

Semiconductor colloidal quantum dots (CQDs) are being increasingly exploited in electronics, optoelectronics and solar energy harvesting, using a variety of different architectures, mostly based on ordered 2D or 3D arrays of these nanostructures. A crucial issue for optimising the performance of such devices is the ability to predict and tune the transport properties of these assemblies. In this work we provide general guidelines to precisely that effect, indicating specific materials, crystal structures, lattice arrangements, surface stoichiometries and morphologies which favour high electron mobilities in these systems, and, conversely, materials that will exhibit low mobilities if nanostructured. At the same time our results evidence a surprising independence of the film's transport properties from those of the bulk material from which the dots are made, highlighting the crucial role of theoretical modelling to guide device design.

Keywords: transport, nanocrystal quantum dots, films, dot arrays, pseudopotential method

Colloidal quantum dots (CQDs) are attractive material systems characterized by outstanding properties, such as low manufacturing costs, high degree of uniformity and flexibility achieved in their synthesis, size-tunability of their electronic and optical properties, and even the ability to engineer their wave functions, enabling unprecedented control of the carriers' localization, that make them potentially ideally suited for a wide range of technological applications. Nevertheless the performance of CQD-based electronic and optoelectronic devices is still far from optimal, owing mainly to the poor transport properties displayed by their building blocks when arranged in arrays. The presence of countless interfaces, with associated traps¹ and potential steps, that the charge carriers need to cross in order to reach the electrodes where they can be collected, appears a daunting obstacle to efficient transport in these devices. Indeed measurements on early devices seemed to confirm this bleak scenario, and very low mobilities (of the order of $10^{-2}\text{cm}^2\text{V}^{-1}\text{s}^{-1}$ or less) were reported in CQD films.²⁻⁵ These findings were supported by

various theoretical models that predicted transport to occur through inefficient phonon-assisted (or 'hopping') conduction⁶⁻¹⁰ or direct tunnelling,^{2-4,11} leading to poor carrier mobility in these systems. Nevertheless surprisingly high mobilities were reported lately by several groups,¹²⁻¹⁸ in high quality films made of different materials, suggesting that band-like transport through extended states is indeed achievable in CQD arrays, provided the surface traps are effectively passivated¹⁸⁻²⁵ and the separation between dots is reduced sufficiently by the use of extremely short ligands or inorganic capping.²⁶ This hypothesis is supported by the observed temperature dependence of mobility and conductivity¹²⁻¹⁸ whereas the spectral broadening and red shifts of the 1S exciton peak observed in these systems,^{13,27} may be indicative of strong electronic coupling between QDs, as are the remarkable values of diffusion lengths and lifetimes of charge carriers measured in QD solids.²⁸

In this work, we carried out a comprehensive and systematic study of the electronic structure and transport properties of CQD films made of different semiconductor materials, representatives of groups III-V, II-VI, and IV-VI, having different bulk crystal structures, varying from zinc blende to wurtzite to rocksalt, considering building blocks (dots) of different sizes, surface morphologies and stoichiometries, placed at different distances from each other and ordered according to different lattice types.

Our results evidence a surprising independence of the film's transport properties from those of the bulk material from which the dots are made, and indicate a strong influence of the dot's structural characteristics (crystal structure, stoichiometry and surface morphology) on the resulting film mobilities. These findings provide invaluable general guidelines to engineer the electron mobility in these systems. Finally, our calculated electron mobilities for CQD films of different materials are consistent with those recently reported in the literature.^{13,17}

We consider 2D arrays of identical, nearly-spherical, perfectly passivated CQDs arranged in an ideal square or hexagonal lattice, as depicted in Figure 1 (in the former the

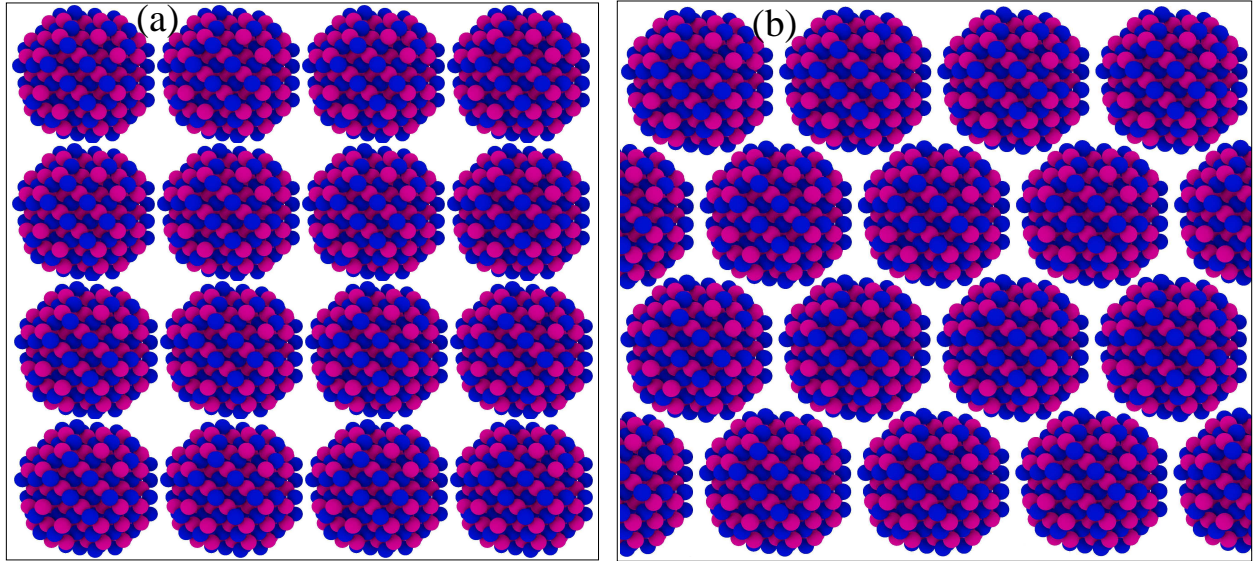


Figure 1: Two-dimensional lattices considered in this work: (a) square lattice and (b) hexagonal lattice. The passivants are not shown.

dots face each other across the $\langle 100 \rangle$ facet, whereas in the latter across the $\langle 110 \rangle$ facet), and we include only nearest neighbor interactions. We therefore neglect the effects of trap/surface states, of thermal vibrations of the dots around their position (positional disorder) and of potential mutual re-orientation of the dots. The electronic structure of such CQD films is modelled using the tight-binding approach, traditionally employed in the modelling of semiconductor bulk solids,^{29,30} with the difference that the atomic orbitals and energies used in the latter are replaced here by the wave functions (and eigenenergies) of the isolated CQD states, obtained within the framework of the atomistic semiempirical pseudopotential method.³¹

We focus on the lowermost miniband in the conduction band, i.e., that formed by the 1S state, as it is the one most likely to be involved in (dark) transport in these systems. Nevertheless, we include up to 15 states in its calculation (i.e., we diagonalize a 15×15 matrix, including states laying few hundreds of meV above the 1S state), to account for possible coupling effects to higher energy bands. All our states are doubly degenerate, when pseudo-spin is included.

The resulting band structures for CQD films made of all the different materials con-

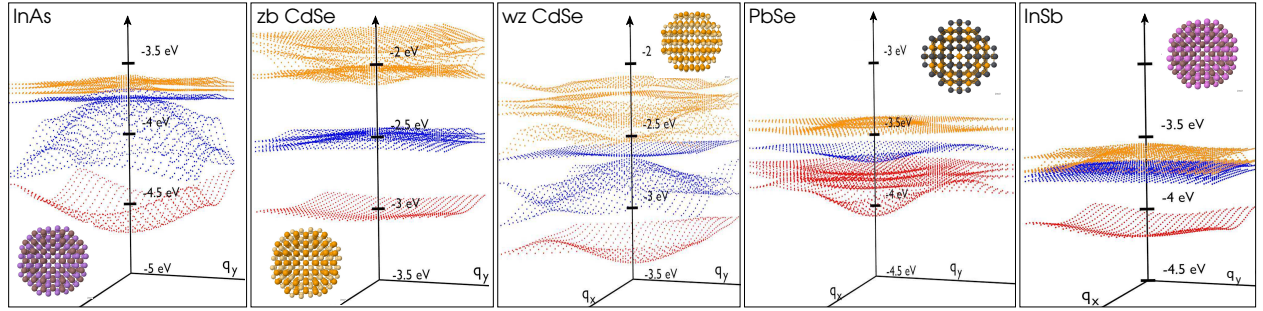


Figure 2: Calculated 3D band structure for CQD films made of different materials (InAs - $R = 1.22$ nm and an As-rich surface -, zinc blende CdSe - $R = 1.22$ nm and a Cd-rich surface-, wurtzite CdSe - $R = 1.26$ nm-, PbSe - $R = 1.26$ nm - and InSb - $R = 1.31$ nm -, all for a dot-to-dot separation $d = 1$ bl. States with the same symmetry have the same color: red for the s-like ground state, blue for the p-like states, and orange for the d-like states. The inset in each panel displays the atomistic structure of the dots considered: brown spheres represent In atoms, violet As, pink Sb, yellow Cd, orange Se, and dark grey Pb.

sidered is shown in Figure 2, for dots with $R \approx 1.2$ nm and a dot-to-dot separation d of one bond length ($1 \text{ bl} = a_0\sqrt{3}/4 = 0.26$ nm for InAs and zinc-blende CdSe, where a_0 is the bulk lattice constant). This is the shortest distance considered in this work.

Our results show that at this separation there is considerable inter-dot coupling in many materials, leading to the formation of several sets of wide minibands. This can be fully appreciated by considering Figure 2, which offers a 3D picture of this effect, where minibands corresponding to states with the same prevalent angular momentum have the same color (red for the s-like ground state; blue for the 3 p-like states and orange for the d-like states).

We find that the inter-dot coupling $V_{ii} = \langle \psi_i(r) | V(r) | \psi_i(r - r') \rangle$ (Figure 3a) decreases exponentially with distance for all materials, in agreement with the results of a previous work on arrays of CdSe dots.³² This effect is shown in Fig. S1 (Supporting Information) for the case of films of InAs CQDs with $R = 1.22$ nm, where the effective masses calculated using Eq. (2) are shown, together with the corresponding miniband widths, as a function of dot-to-dot separation d .

Given the extreme sensitivity of the film's band structure to the inter-dot separation found here, it is important to determine what can be considered as a realistic value for d .

A strong dependence of carrier mobility on the ligand length has also been established in several recent experimental studies^{26,28,33} (although there are also indications³⁴ that the nature of the dot-ligand interaction is not always solely geometrical, but can also involve electronic coupling,³⁵ with non-trivial consequences on the film's mobility. This is especially true in the case of inorganic, i.e. halide, passivation).

The presence on the CQD surface of native bulky passivants limits their proximity and represents a barrier to efficient charge transport between dots. The inter-particle separation can however be reduced, and the electronic coupling between CQDs enhanced, by exchanging them for shorter ligands,³⁶ or by removing them altogether via thermal annealing.^{37,38} The length of the capping agents routinely employed to stabilize the surface of these nanostructures ranges from 2 nm for oleic acid,³⁹ to 0.35 nm for oxalic acid.²⁸ The use of inorganic ligands, such as atomic halide anions (Cl^- , Br^- and I^-), can lead to a further decrease of the inter-dot separation in a film down to 0.1 nm.²⁰ Furthermore, after undergoing reactive self-assembly^{40–42} or laser annealing,⁴³ the dots can bond facet-to-facet preserving both crystalline atomic ordering across the interface and long range order across the film and even form coherent percolative networks.⁴⁴ All this experimental evidence supports our choice of $d = 1$ bl (> 0.2 nm) as an inter-dot separation realistically achievable in technologically relevant CQD films.

Starting from the calculated band structure, we extract miniband widths W_i (Figure 3b) and effective masses m_i^* (Figure 3c). The latter are calculated in two independent ways: (i) by fitting the calculated band structure around $q=0$ with a parabola

$$m_i^* = \frac{\hbar^2 q_i^2}{2(E_i - E_0)} \quad (1)$$

where E_i is the calculated energy at $q = q_i$ (for q_i close to 0), and E_0 is the energy at $q = 0$, and then taking the arithmetic average of the effective masses obtained along two perpendicular in-plane directions $i = x, y$ (Figure 3c, blue bars), and (ii) by using the approximate

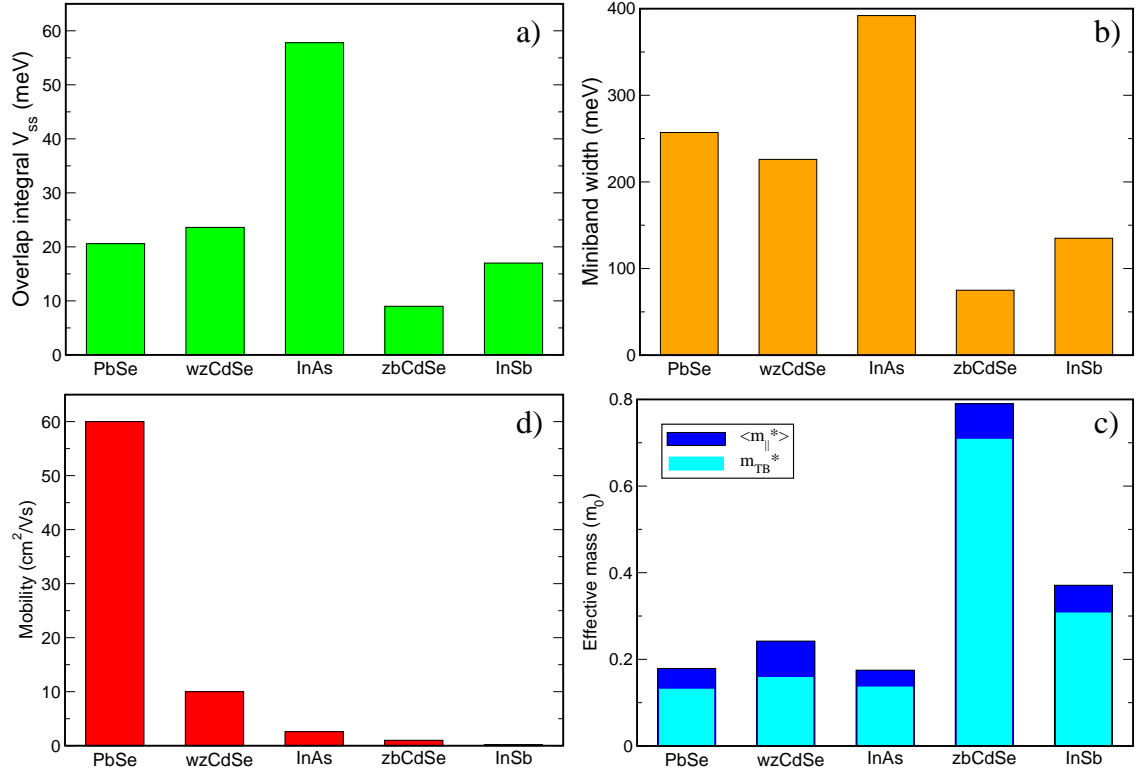


Figure 3: Calculated overlap integrals $V_{ss} = \langle \psi_s(r) | V(r) | \psi_s(r - r') \rangle$ (a), miniband widths (b), effective masses at Γ - using both Eq. (1) and Eq. (2) - (c), and mobilities (d), relative to the lowermost miniband, for an inter-dot spacing of 1 bl, in CQD films of different materials (see Figure 2).

tight-binding expression (Figure 3c, cyan bars)

$$m_i^*(q=0) = \frac{\beta_i \hbar^2}{W_i a^2} \quad (2)$$

where β_i is a constant that depends on the specific lattice and state i , and $a = 2R + d$ is the center-to-center distance between nearest-neighbor CQDs (more details can be found in the Supporting Information). The results are presented in Figure 3 and Table 1, for $d = 1$ bl.

Table 1: Calculated overlap integrals (V_{ss}), miniband widths (W) and effective masses at Γ (m_x^* and m_y^* are obtained along x and y by fitting the miniband curvature around $q = 0$ with a parabola, according to Eq. (1), $\langle m_{\parallel}^* \rangle = (m_x^* + m_y^*)/2$, is their arithmetic average, whereas m_{TB}^* are calculated using Eq. (2) at $d = 1$ bl, for different materials, radii (R), and surface terminations (CdSe dots in the wurtzite phase exhibit ‘mixed’ surfaces, with no clear prevalence of a specific atomic species at the interface with the neighboring dots). δR represents the threshold size distribution that satisfies $V_{ii} = \Delta E = |E_i(R) - E_i(R \pm R\delta R/100)|$, at which Anderson localization effects start to occur († for wz CdSe and InSb two values for δR are reported, as the E_i vs R curve is not a straight line in this case, but has a different slope in the direction of larger sizes [first value in column 4] from that towards smaller sizes [second value in column 4]).

Material	2D Lattice	Surface	R[nm]	δR [%]	V_{ss} [meV]	m_x^*	m_y^*	$\langle m_{\parallel}^* \rangle$	m_{TB}^*	W [meV]
InAs	square	a-rich	1.22	2.5	57.8	0.181	0.169	0.175	0.136	392
InAs	square	c-rich	1.22	2.5	17.1	0.445	0.445	0.445	0.394	136
CdSe(zb)	square	a-rich	1.22	<1	8.0	0.863	0.862	0.863	0.793	67
CdSe(zb)	square	c-rich	1.22	<1	9.0	0.807	0.774	0.790	0.708	75
CdSe(wz)	hex.	mixed	1.26	4, 2.3 †	23.6	0.282	0.201	0.242	0.157	226
CdSe(wz)	square	mixed	1.26	4, 2.3 †	23.6	0.395	0.281	0.338	0.235	204
PbSe	hex.	c-rich	1.26	2	20.6	0.159	0.199	0.179	0.131	257
InSb	square	a-rich	1.31	20, 1.5 †	17.0	0.350	0.392	0.371	0.307	135
InAs	square	a-rich	1.99	n/a	5.9	0.453	0.441	0.447	0.420	49
CdSe(wz)	hex.	mixed	1.92	1.7, 2.6 †	9.0	0.261	0.449	0.355	0.192	78

Since our 2D arrays are made of *identical* CQDs, another important point is to determine to what extent this condition is responsible for the formation of wide minibands with their associated small effective masses, in close packed films, or, in other words, how resilient the conditions for bulk-like transport are in a realistic situation of dots chemi-

cally synthesized in the lab. The main issue here is Anderson's localization,⁴⁵ the most likely origins of which have been identified⁴⁶ to be (i) size and (ii) positional disorder. Localization occurs when the energy broadening caused by disorder is larger than the coupling between neighboring sites V_{ii} ($i = s, p, d, \dots$ is the angular momentum of the dots' wave functions). Our present model is unfortunately unable to estimate the energy spread due to fluctuations in the dot position. We will therefore address the effects of size distribution on the realization of the conditions for bulk-like transport. Indeed it has been recently pointed out⁴⁷ that this is probably the main source of energy fluctuations in arrays of CQDs. The energy spread due to size distribution ΔE must satisfy $\Delta E_i < V_{ii}$ for the array to be free from localization effects due to size fluctuations. Our calculated overlap integrals for the 1S state, V_{ss} , are presented in Figure 3a and Table 1, where the corresponding values for the size distribution are also shown. In films of InAs CQDs, for example, $V_{ss} = 58$ meV for $d = 1$ bl and $V_{ss} = 18.5$ meV for $d = 1.6$ bl (not shown in Table 1). This corresponds to size distributions $< 2.5\%$, and $< 1\%$, respectively. While the former could be achievable with modern growth methods, the latter is not within their reach yet. Some localization effects caused by size variations could therefore be expected in films of small ($R \sim 1.2$ nm) InAs CQDs separated by more than 1 bl for transport in the lowest miniband.

The widest ground state miniband, with one of the smallest associated effective masses, is found in InAs. Interestingly a film of zinc-blende CdSe CQDs with the exact same total number of atoms as the InAs dots and, due to the similarity of the lattice constants between the two materials - 0.6058 nm vs 0.6081 nm - also essentially the same size [$R(\text{InAs})=1.220$ nm vs $R(\text{CdSe})=1.225$ nm, as calculated based on the total number of atoms and assuming a spherical shape⁴⁸], exhibits 1S miniband widths (effective masses) a factor of over 5 narrower (larger). This effect can be attributed to the different values of the electron effective masses in the two bulk materials. Indeed it has been observed³² that all the effective parameters, including hopping terms and bandwidths, scale as the

inverse of the bulk effective mass.

The same is not true, however, for the third (1d) miniband, which exhibits a width of about 300 meV at 1 bl, as a result of the coupling of up to 6 states. This coupling persists for separations of 1.3 bl (when the band width decreases to about 210 meV), but is broken at 1.6 bl, when the lowermost doublet decouples from the higher energy multiplet of four states. The latter forms a miniband whose width (~ 135 meV) is similar to that of the 1S and 1P bands calculated for InAs dots of the same size at the same distance. Efficient transport could therefore be achievable in zinc-blende CdSe CQDs even at this separation, provided the doping level is high enough so that this high band can be populated.

According to the *effective mass rule*³² mentioned above, wider minibands and smaller associated effective masses are expected for 2D arrays of CQDs made of materials with small bulk effective masses. We tested this hypothesis in the case of InSb, whose bulk effective mass is a factor of ~ 2 smaller than that in InAs, and therefore promises miniband widths of the order of ~ 800 meV. Furthermore this material exhibits, in the bulk, the highest electron mobility among all semiconductors, and is therefore a good candidate for testing transport properties at the nanoscale. The results, displayed in Figure 3 and Table 1, contradict these expectations, exhibiting widths about 1/3 of those calculated in the case of InAs dots with the same number of anions and cations (however slightly different in size, owing to the different lattice constant between InSb and InAs), and effective masses over 2 times larger. The origins of this surprising behavior are unclear. We suggest that they may be related to the peculiar electronic structure of *small* InSb CQDs, where a k-space decomposition analysis of the conduction band minimum (CBM) wave function recently evidenced⁴⁹ a large contribution from the L-point in the Brillouin zone, in contrast to the case for InAs dots of the same size. The presence of such high-frequency components could adversely affect the overlap integrals and therefore the miniband effective masses.

Another very interesting material from the application point of view, owing to its ex-

tensive exploitation in next generation CQD-based solar cell devices, is PbSe. As its peculiar electronic structure, with a direct band gap situated at the L point in the Brillouin zone,⁵⁰ yields 8-fold degenerate band edges in the bulk, arrays of CQDs of this material may have the potential to form very wide minibands. Indeed, it is easy to show that, according to the tight-binding model, a lattice made of dots with an N-fold degenerate 1S-type spherically symmetric identical ground state results in an (N-1)-fold degenerate, perfectly flat band plus a single band at lower energies, whose width is N times the width exhibited by the lowest miniband in an array of dots with a *single*, non-degenerate 1S ground state, arranged in the same lattice. Considering that in a PbSe CQD the 8-fold degeneracy of the bulk band edge states is lifted,⁵⁰ leaving a two-fold degenerate ground state (4-fold including spin) and two singly-degenerate higher levels (doubly-degenerate with spin), and that the wave functions of these states are not exactly the same, our findings of 3 nearly flat bands with slightly different energies, plus a 260 meV wide ground state (Figure 2) are consistent with the tight-binding predictions.

Experimentally, films of PbSe CQDs have been observed to assemble in square,⁴² honeycomb⁴² and hexagonal⁵¹ lattices. In Figure 2 we present the band structure calculated assuming an hexagonal configuration. Our results show that films of CQDs made of PbSe exhibit the smallest effective mass and one of the largest miniband widths of all materials considered (see Figure 3 and Table 1): these systems are therefore potentially ideally suited for a wide variety of optoelectronic applications requiring good transport properties.

An interesting question is whether the transport properties of a material are affected by its crystal structure and, if so, to what extent. The band structure parameters calculated for films made of zinc blende and wurtzite CdSe CQDs (the latter are assumed to be arranged either in an hexagonal lattice, with their c axis aligned perpendicular to the film plane, or in a square lattice), of similar sizes (1.22 nm and 1.26 nm, respectively) can be compared in Figure 2, Figure 3 and Table 1. The wurtzite structure clearly outperforms

zinc-blende in terms of transport, exhibiting a 1S miniband width a factor of ~ 3 wider than the zinc-blende phase (and effective masses about the same factor smaller) for the closest inter-dot separation. It is clear, however, that the 1S miniband width of wurtzite CdSe CQDs remains smaller than that obtained in the case of similarly sized InAs dots. As the bulk effective masses of CdSe are nearly the same in both the cubic and the hexagonal modification, this large difference in transport properties represents another violation of the simplistic *effective mass rule*.

A further question arises regarding the effect of the different lattice arrangements of the dots (square vs hexagonal) on the array's band structure. Our results for films of wurtzite CdSe dots predict better transport properties for hexagonal (hex) lattices, compared to square (sq) ones, (provided that the dots are the same and their separation is the same in both arrays), and yield a miniband effective mass ratio $m_{\text{sq}}^*/m_{\text{hex}}^*$ of 1.4, in good agreement with the standard tight-binding theory, which, in the case of perfectly decoupled bands, predicts (see Eq. S1 in the Supporting Information) the ratio of the miniband effective masses in 2D square and hexagonal lattices to be 1.5, i.e., inversely proportional to the ratio of the number of nearest neighbors in the two arrangements (4/6).

The transport properties of CQD films are also found to be strongly size dependent, and more markedly so for III-V materials: two examples - InAs and wurtzite CdSe - are provided in Table 1 (further details on the size-dependence of the band structure parameters can be found in the Supporting Information). In the former material, the miniband widths of 2D arrays of CQDs with $R = 1.99$ nm are a factor of about 8 narrower than those obtained for dots with $R = 1.22$ nm, (and the effective masses about 3 times heavier), whereas in the case of CdSe, the difference in miniband width between films of dots with $R = 1.26$ nm and $R = 1.92$ nm drops to a factor of about 3 (1.5 for the effective masses). This size-dependence is due to a reduction in the overlap integral with increasing dot size, an effect common to all materials, result of the space normalization of the isolated-dot wave functions (i.e., the fact that, as the overall probability of finding the

electron anywhere in the dot - given by the integral over the dot volume of the wave function squared - is 1, the probability of finding it at any specific location within the dot - given by the amplitude of the wave function at that location - decreases with increasing dot volume).

Given that, as we have seen, the inter-dot separation is a crucial parameter determining the width of the minibands and the magnitude of the associated effective masses, an interesting question is whether the *details* of the surfaces of the nanostructures facing each other have any influence on the strength of their coupling, hence on the electronic structure of the 2D array. Figure S2 (Supporting Information) compares the miniband widths and effective masses calculated for films of InAs dots with the same nominal size ($R=2$ nm) but with slightly different surface morphologies: in case (i) the surfaces facing each dot terminate with a flat facet of In atoms; in case (ii) these surfaces have two added As atoms, and have therefore a "bumpy" profile; finally, in case (iii) the two As atoms on the surface of one dot interlock with the atoms on the surface of the other, like two LEGO bricks (Although cases (ii) and (iii) may seem artificial and perhaps unrealistic, they allow us to investigate the effects on the film's electronic structure and mobility of some degree of surface roughness that may be found in experimental samples). We find that the miniband width in cases (i) and (ii) scales with the number of outermost surface atoms (i.e., those facing each other at the dot-to-dot interface), whereas in case (iii) it is enhanced compared with case (i), due to the enhanced coupling caused by the interdigitation (this effect is highlighted by the non-exponential behaviour of both width and effective masses for negative distances - see first point in the red curves of Figure S2 (Supporting Information)). These results highlight the importance of a clean flat surface in order to obtain strong inter-dot couplings and good transport properties. However, they also suggest that even stronger couplings are achievable in interlocked dots, indicating possible new strategies to enhance transport in these systems.

Taking the surface argument further, we may ask ourselves whether also the atomic

species terminating the surface may influence the strength of the interdot coupling in a 2D array. We investigated this effect by comparing the electronic structure calculated for films made of InAs and zinc blende CdSe dots with $R=1.22$ nm with anion- and cation-terminated surfaces. In both InAs and zinc blende CdSe dots the total number of atoms is the same (275) and the number of anions and cations in each is almost identical (140 vs 135). Our results (Table 1 and Fig. S1 - Supporting Information) exhibit, however, a strikingly different behavior in the two materials: anion-terminated structures yield stronger coupling, hence better transport properties, in InAs, whereas the opposite is true for zinc blende CdSe. This effect is, however, much stronger in arrays of InAs dots, where the enhancement is three-fold, than in zinc blende CdSe films, where the variation in the coupling is just 10%.

Once more the surface *details* are found to have a profound influence on the dot-to-dot interactions in multidimensional arrays.

All the quantities in Figure 3a, b, and c are consistent, so that the material with the largest interdot coupling (InAs, Figure 3a) also exhibit the widest miniband (Figure 3b) and the smallest effective mass (Figure 3c), and, *vice versa*, films of zinc blende CdSe, where the coupling is weakest, have the narrowest miniband and the largest effective masses. The same is however not true for the mobility (Figure 3d): surprisingly there is little relationship between the electron effective mass and its mobility within a miniband.

Assuming that the electrons are scattered by fluctuations in the dot size alone,⁴⁷ we derive the following expression for an order-of-magnitude estimate of the mobility in the lowest miniband of a CQD film⁵²

$$\mu_{OM}(\rho_{\text{defects}}, \delta R) = \frac{e\hbar^3}{m^{*2}\rho_{\text{defects}}MA} \quad (3)$$

where e is the electron charge, ρ_{defects} is the density of scattering centers (i.e., defect dots with radius $R - \delta R$), M depends on the scattering potential, A is the unit cell area, and m^*

is the effective mass of the miniband obtained using Eq. (1) (further details are available in the Supporting Information).

According to these estimates, mobilities $\sim 1 \text{ cm}^2 \text{ V}^{-1} \text{ s}^{-1}$ are achievable in CQD arrays of almost all materials considered. This is an important threshold for achieving rapid exciton dissociation for PV applications. Indeed it has been shown³³ that for mobilities in excess of $1 \text{ cm}^2 \text{ V}^{-1} \text{ s}^{-1}$, all photogenerated electron-hole pairs separate rapidly enough to escape Auger recombination and the carrier multiplication efficiency in CQD films approaches the value observed in dot dispersions.

Table 2: Order-of-magnitude [a] and maximum [b] in-plane dark mobilities (in $\text{cm}^2 \text{ V}^{-1} \text{ s}^{-1}$) calculated at room temperature for "touching dots" using Eq. (3) [a] and Eq. (4) [b] (as this expression was derived for cubic lattices, the mobility was rescaled by a factor of 1.5^2 in the case of hexagonal lattices to account for the difference in the miniband effective masses in the two configurations - see text), for different materials, dot radii and surface terminations (CdSe dots in the wurtzite phase exhibit 'mixed' surfaces, with no clear prevalence of a specific atomic species at the interface with the neighboring dots). The values for the electron confining potentials (U_0) and assumed size distribution (χ) are also reported (the calculated overlap integrals V_{ss} are listed in Table 1), Owing to the atomistic nature of our approach, it was difficult to achieve the same relative size difference for all dots, and it was impossible to obtain values lower than 8%, while keeping a nearly spherical shape, when most of the CQDs radii were close to 1.2 nm. This is why we used similar but different values for χ for different materials and dot sizes. For ease of comparison with the results of ref.,⁴⁷ the mobilities calculated with Eq. (4) using a 5% size distribution are also reported (in brackets) next to those obtained for the different values of χ reported in the third column. A 1% density of defects was assumed in Eq. (3).

Material	Lattice	Surface	R[nm]	U_0 [eV]	χ [%]	$\mu_d^{OM[a]}$	$\mu_d^{max[b]} (\chi = 5\%)$
PbSe	hex.	c-rich	1.26	4.56	9.2	65	1.8 (6.1)
CdSe(wz)	hex.	mixed	1.26	3.59	10.4	11	3.1 (13.7)
CdSe(wz)	square	mixed	1.26	3.59	10.4	4.7	1.4 (6.1)
InAs	square	a-rich	1.22	5.16	8.4	2.6	9.2 (26.0)
InAs	square	c-rich	1.22	5.16	8.4	0.8	0.4 (1.2)
CdSe(zb)	square	c-rich	1.22	3.48	8.5	1.0	0.2 (0.6)
CdSe(zb)	square	a-rich	1.22	3.48	8.5	0.7	0.1 (0.4)
InSb	square	a-rich	1.31	4.75	8.6	0.2	0.6 (1.6)
CdSe(wz)	hex.	mixed	1.92	3.59	7.6	5	1.3 (2.9)
InAs	square	a-rich	1.99	5.16	8.0	0.4	0.1 (0.2)

An alternative approximate expression for the dark mobility in a simple cubic 3D su-

percrystal, valid under the assumption that fluctuations in the size of the CQDs represent the main source of electron scattering (small radius limit $qR \ll 1$), was recently derived within the framework of the $k \cdot p$ approach by Shabaev, Efros and Efros.⁴⁷ In the case of touching dots this reduced to⁴⁷

$$\mu_d^{max} = \frac{2^8}{3\pi^{3/2}} \frac{eR^2}{\hbar} \frac{t^{5/2}}{\chi^2 U_0^2} \frac{1}{\sqrt{k_B T}} \quad (4)$$

where t is the overlap integral, χ the size dispersion, U_0 the confining potential for the electrons, T the temperature and k_B the Boltzmann constant. As the in-plane overlap integrals are independent of the dimensionality of the array, we can substitute in Eq. (4) our calculated values for $V_{ii} = t$ and U_0 (also reported in Table 2) to obtain estimates for the maximum in-plane dark mobilities achievable in arrays of CQDs of different materials, according to Eq. (4). A comparison between the predictions of the latter and those obtained using our approach (Eq. (3)) is presented in Table 2 (as (4) was derived for cubic lattices, the mobility in the last column of the table was rescaled by a factor of $(m_{sq}^*/m_{hex}^*)^2 = (3/2)^2$ in the case of hexagonal lattices - PbSe and wzCdSe - to account for the difference in the miniband effective masses in the two configurations, see below).

We find (Figure 3d, and Table 2) that the mobility exhibits strong variations from material to material (when considering dots with the same size), from crystal structure to crystal structure (when considering dots of the same material), from lattice type to lattice type (when considering dots of same size, material and crystal structure), and from size to size (when considering dots of the same material and crystal structure): arrays of PbSe CQDs exhibit the highest mobilities, consistent with the values recently observed in these systems,¹⁷ whereas, surprisingly, the lowest values are obtained for InSb, which boasts, instead, the highest mobility of all semiconductors in the bulk (if compared with films of InAs dots, with which they share very similar material properties, the main origin of the low mobility predicted for arrays of InSb CQDs is the large value of their effective mass);

the mobility in CdSe films is about 5 times larger for dots in the wurtzite phase than for those in the zinc blende crystal structure, despite the significant difference in size distribution between the two films where $\chi(\text{wz}) > \chi(\text{zb})$;⁵⁵ 2D hexagonal lattices exhibit larger mobilities than square ones, mainly owing to the difference in their respective miniband effective masses (with $m_{\text{sq}}^* \approx 1.5m_{\text{hex}}^*$), leading to an increase by a factor of $\sim 1.5^2 = 2.25$ (due to the m^{*-2} dependence in (3)) in the mobility of hexagonal lattices (the ratio between the mobilities we calculate in hexagonal and square lattices of wurtzite CdSe QDs is indeed 2.3); finally, arrays of InAs dots of different sizes ($R = 1.2$ nm vs $R = 2.0$ nm) display larger differences in mobility (about a factor of 6) compared to films of similarly sized wurtzite CdSe dots (where larger structures exhibit mobilities only a factor of 2 smaller). In particular we found that arrays of wurtzite CdSe QDs with $D = 3.8$ nm can exhibit mobilities of the order of ~ 12 cm² V⁻¹s⁻¹, if the dots are placed at a distance of 1 bl (0.26 nm) and have a size distribution of 5% (data not shown in Table 2, where we report our results for $\chi = 7.6$ for a fairer comparison with the other sizes and materials). These estimates are consistent with the dark mobilities (27 cm² V⁻¹s⁻¹)¹³ observed experimentally in these systems, and in sharp contrast to the predictions of Eq. (4), which yields (when the resulting mobility is multiplied by a factor of 2.25 to account for the different - i.e. hexagonal - lattice type), for the same system, a *maximum achievable mobility* over a factor of 4 smaller than ours and nearly one order of magnitude smaller than experiment. Similarly, in the case of films of “touching” PbSe QDs with $D = 2.52$ nm (and a size distribution of 9%) we predict mobilities around 65 cm² V⁻¹s⁻¹ (vs 1.8 cm² V⁻¹s⁻¹, using Eq. (4) adjusted for an hexagonal lattice), which are in good agreement with recently reported electron mobilities¹⁷ (10 cm² V⁻¹s⁻¹), if considering that the latter were obtained in films made of larger dots ($D = 6$ nm) and with a narrower size distribution. Interestingly the experimental samples where such record-high mobilities were observed had a Pb-rich surface, like the dots considered here (see inset of panel 4 in Figure 2), where the ratio of Pb to Se atoms is about 1.2. Even higher electron mobilities can be achieved in

PbSe films when the dots are 'fused' together and connected by necks with thicknesses close to the dots' diameters, forming percolative networks.⁴⁴ However, as such systems exhibit uninterrupted segments of attached CQDs, whose length may even approach the distance between electrodes, their transport properties are very different from those of the films considered in the present work, where the dots do not touch.

In comparing our results with those of Shabaev *et al.*,⁴⁷ it is worth pointing out that, unlike in ref.,⁴⁷ here we do not treat U_0 as a fitting parameter. As in the calculation of the isolated dot wave functions we take the vacuum level as a reference zero energy, for a meaningful comparison between the results of Eq. (3) and Eq. (4), the depth U_0 of the electron well (see Table 2) is determined consistently within the atomistic semiempirical pseudopotential framework, i.e., as the absolute value of the calculated position of the conduction band, in the limit of infinitely large dots (which is in good agreement with the asymptotic behavior observed in recent accurate photoelectron spectroscopic measurements⁵³). Any reduction in the electron confinement would lead to a substantial increase in the mobilities, owing to the combined effect of an increase in the overlap integral t (raised to the power of 5/2 in the numerator of Eq. (4)) and a decrease of U_0 (raised to the power of 2 in the denominator of Eq. (4)). As an example, a reduction of 0.5 [1.0] eV in U_0 alone (i.e., without considering the corresponding increase of the overlap integral $t = V_{ss}$) would lead to a 25% [54%] increase in the mobility calculated for an array of InAs dots with $R=1.2$ nm. In this respect, we note that in order to reproduce the experimental dark mobilities measured in ref.,¹³ Shabaev and Efros must assume unrealistic values for U_0 (i.e., < 1 eV), which are more suitable to epitaxial dots, than colloidal nanostructures. This is because the continuum-like approach of ref.⁴⁷ largely underestimates the overlap integrals t . Indeed, in order to obtain the same values for t we calculated for arrays of touching wurtzite CdSe CQDs (see Table 1), Shabaev and Efros need to assume a confining potential about 3 eV smaller (0.6 eV) than the one used in our atomistic approach (compare Table 1 and Fig.2e in ref.⁴⁷).

Furthermore, while the mobility in Eq. (3), together with an inverse dependence on the size difference between nominal-size dots and scatterers (expressed through the matrix element M), also exhibits a crucial inverse dependence on the density of the scattering centers, as one would expect, Equation (4) only accounts for the former through the size dispersion χ , but lacks any explicit dependence on the latter. On the other hand, unlike in Eq. (4), there is no temperature dependence in Eq. (3), consistently with the expected temperature independence of the scattering mechanism considered in this work, where the defect density does not depend on temperature.⁵⁴

In our investigation we find that the value of the mobility is influenced by many different factors, among which the miniband's effective mass represents an important - but not the only important - contribution. A paramount role is played by the material, and by that we mean the nanoscopic details of the atomic potentials, as ΔV (the perturbation in the potential due to a difference in dot size, which appears in the integrals in the mobility calculations Eq. (3), in the case of size-fluctuation-governed scattering), can vary by orders of magnitude between two different materials, even when the QDs have the same configuration at the atomic level, as in the case of InAs and zinc-blende CdSe dots (which have the same number of atoms arranged in nearly identical positions). The magnitude and symmetry of the electron wave functions in the region where ΔV is non-zero are also crucial to the evaluation of the mobility integrals. It is therefore difficult to infer relative values for the mobility of different materials simply based on their respective miniband effective masses (which depend on the value of the overlap integral $\langle \psi_i(r) | V(r) | \psi_i(r - r') \rangle$ - a fundamentally different quantity from the perturbation integral $\langle \phi_i(r) | \Delta V(r) | \phi_i(r) \rangle$), as the results presented in Table 2, Table 1 and Figure 3 confirm. Indeed, the above factors sometime combine to yield unexpected results, such as in the case of PbSe or zinc-blende CdSe (where the former, despite having an effective mass similar to InAs, exhibits a mobility over 22 times larger, and the latter, with an effective mass over 5 times heavier than InAs, shows a similar mobility), depending on the relative weight of their separate con-

tributions. It is important to stress that, owing to its distinctive features, this effect can only be captured within the framework of an atomistic approach and is therefore beyond the reach of continuum-like methods, such as the popular $k \cdot p$ approach.

We should also mention here that, as our single-dot calculations are performed in vacuum (which condition places the strongest constraints on the extension of the wave functions outside the dot, hence on the magnitude of inter-dot coupling), our estimates for miniband widths [effective masses] and associated mobilities represent lower [upper] limits for these quantities.

In conclusion, we investigated the effects of size, crystal structure, material composition, stoichiometry, surface morphology and dot-to-dot separation on the band structure parameters and electron mobilities in CQD films. Our results evidence a surprising independence of the film's transport properties from those of the bulk material from which the dots are made, and indicate a strong influence of the dot's structural characteristics (crystal structure, stoichiometry and morphology) on the resulting film mobilities. InAs dots exhibit the widest minibands, with associated smallest effective masses, however the largest mobilities of all materials considered - of the order of tens of $\text{cm}^2 \text{V}^{-1}\text{s}^{-1}$ - are found in PbSe (these values are consistent with the highest mobilities recently reported for thin films of PbSe CQDs¹⁷), whereas 2D arrays of InSb dots are predicted to exhibit the lowest mobility of all materials considered, despite the record-high mobility observed in that material in the bulk. By comparing 2D arrays made of the same material but with different crystal structures, we show that wurtzite outperforms zinc-blende in terms of transport properties, exhibiting mobilities about one order of magnitude larger. Our calculated mobilities for 2D arrays of wurtzite CdSe dots are also consistent with recent experimental measurements.¹³ Our results further show that smaller dots exhibit stronger coupling, hence wider minibands and higher mobilities. A crucial aspect determining the coupling strength between adjacent dots is found to be their surface morphology: well defined (i.e., flat) facets, where a large number of perfectly aligned atoms face each

other across the inter-dot gap, provide the best interface for strong dot-to-dot interaction, whereas in the presence of rough surfaces, where a few adatoms protrude from the surface, the extent of wave function overlap is limited to these few atoms, reducing the overall electronic coupling (which is proportional to the number of atoms on the surfaces facing each other), for the same nominal inter-dot separation and dot size. Interestingly we find that stoichiometry also plays an important role in determining the transport properties of dot arrays. This effect is found to be stronger in III-V materials than in II-VI. Our results also highlight a non-trivial relationship between the mobility of an electron and its effective mass within a miniband, that can only be captured by considering the atomistic details of the material and is therefore outside the reach of continuum-like methods, such as the popular effective mass $k\cdot p$ approach. This work represents a crucial step in the effective design and optimisation process of CQD films for specific device applications.

Acknowledgement

M.C. gratefully acknowledges financial support from the Royal Society under the URF scheme, and from GENIL - Strengthening through Short-Visits Ref. GENIL-SSV 2014. F.M.G.C. and S.R.B. were supported by Project TEC2013-47283-R, funded by the Spanish Secretaria de Estado de Investigación, Desarrollo e Innovación, Ministerio de Economía y Competitividad; F.M.G.C. was also funded by Project mP_TIC_5 from Campus de Excelencia Internacional BioTic Granada; and a mobility grant from the "José Castillejo" program for young researchers funded by Spanish Ministerio de Educación, Cultura y Deporte.

Supporting Information Available

Atomistic modelling of single CQDs, Tight-binding band structure parameters, Dependence of the band-structure parameters on the interdot separation, Size-dependence of

the band structure, Effect of different surface morphologies, An order-of-magnitude expression for the mobility This material is available free of charge via the Internet at <http://pubs.acs.org>.

References

- (1) Califano, M.; Gomez-Campos, F. M. *Nano Lett.* **2013**, *13*, 2047-2052.
- (2) Yu, D.; Wang, C.; Guyot-Sionnest, P. *Science* **2003** *300*, 1277-1280.
- (3) Vanmaekelbergh, D.; Liljeroth, P. *Chem. Soc. Rev.* **2005**, *34*, 299-312.
- (4) Kovalenko, M. V.; Scheele, M.; Talapin, D.V. *Science* **2009** *324*, 1417-1420.
- (5) Wehrenberg, B. L.; Yu, D.; Ma, J. S.; Guyot-Sionnest, P. *J. Phys. Chem. B* **2005**, *109*, 20192-20199.
- (6) Chandler, R. E.; Houtepen, A. J.; Nelson, J.; Vanmaekelbergh, D. *Phys. Rev. B* **2007**, *75*, 085325/1-085325/10.
- (7) Yu, D.; Wang, C.; Wehrenberg, B. L.; Guyot-Sionnest, P. *Phys. Rev. Lett.* **2004**, *92*, 216802.
- (8) Liu, H.; Pourret, A.; Guyot-Sionnest, P. *ACS Nano* **2010**, *4*, 5211-5216.
- (9) Chu, I.-H.; Radulaski, M.; Vukmirovic, N.; Cheng, H.-P.; Wang, L.-W. *J. Phys. Chem. C* **2011**, *115*.
- (10) Mentzel, T. S.; Porter, V. J.; Geyer, S.; MacLean, K.; Bawendi, M. G.; Kastner, M. A. *Phys. Rev. B* **2008**, *77*, 075316.
- (11) Talapin, D. V.; Lee, J.-S.; Kovalenko, M. V.; Shevchenko, E. V. *Chem. Rev.* **2010** *110*, 389-458.

- (12) Mentzel, T. S.; Wanger, D. D.; Ray, N.; Walker, B. J.; Strasfeld, D.; Bawendi, M. G.; Kastner, M. A. *Nano Lett.* **2012**, *12*, 4404-4408.
- (13) Choi, J.-H.; Fafarman, A. T.; Oh, S. J.; Ko, D. K.; Kim, D. K.; Diroll, B. T.; Muramoto, S.; Gillen, J. G.; Murray, C. B.; Kagan, C. R. *Nano Lett.* **2012**, *12*, 2631-2638.
- (14) Lee, J.-S.; Kovalenko, M.; Huang, J.; Chung, D. S.; Talapin, D. Band-like transport, high electron mobility and high photoconductivity in all-inorganic nanocrystal arrays. *Nat. Nanotechnol.* **2011**, *6*, 348-352.
- (15) Talgorn, E.; Gao, Y.; Aerts, M.; Kunneman, L. T.; Schins, J. M.; Savenije, T. J.; van Huis, M. A.; van der Zant, H. S. J.; Houtepen, A. J.; Siebbeles, L. D. A. *Nat. Nanotechnol.* **2011**, *6*, 733-739.
- (16) Yang, Y.; Liu, Z.; Lian, T. *Nano Lett.* **2013**, *13*, 3678-3683.
- (17) Oh, S. J.; Berry, N. E.; Choi, J.-H.; Gauldin, E. A.; Paik, T.; Hong, S.-H.; Murray, C. B.; Kagan, C. R. *ACS Nano* **2013**, *7*, 2413-2421.
- (18) Oh, S.; Wang, Z.; Berry, N.; Choi, J.; Zhao, T.; Gauldin, E. A.; Paik, T.; Lai, Y.; Murray, C. B.; Kagan, C. R. *Nano Lett.* **2014**, *14*, 6210-6216.
- (19) Ip, A. H.; Thon, S. M.; Hoogland, S.; Voznyy, O.; Zhitomirsky, D.; Debnath, R.; Levina, L.; Rollny, L. R.; Carey, G. H.; Fischer, A.; Kemp, W. K.; Kramer, I. J.; Ning, Z.; Labelle, A. J.; Chou, K. W.; Amassian, A.; Sargent, E. H. *Nat. Nanotechnol.* **2012**, *7*, 577-582.
- (20) Tang, J.; Kemp, K. W.; Hoogland, S.; Jeong, K. S.; Liu, H.; Levina, L.; Furukawa, M.; Wang, X.; Debnath, R.; Cha, D.; Chou, K. W.; Fischer, A.; Amassian, A.; Asbury, J. B.; and Sargent, E. H. *Nat. Mater.* **2011**, *10*, 765-771.
- (21) Ning, Z.; Voznyy, O.; Pan, J.; Hoogland, S.; Adinolfi, V.; Xu, J.; Li, M.; Kirmani, A. R.; Sun, J.-P.; Minor, J.; Kemp, K. W.; Dong, H.; Rollny, L.; Labelle, A.; Carey, G.;

- Sutherland, B.; Hill, I.; Amassian, A.; Liu, H.; Tang, J.; Bakr, O. M.; Sargent, E. H. *Nat. Mater.* **2014**, *13*, 822-828.
- (22) Zhang, J.; Gao, J.; Miller, E. M.; Luther, J. M.; Beard, M. C. *ACS Nano* **2014**, *8*, 614-622.
- (23) Chuang, C. M.; Brown, P. R.; Bulovic, V.; Bawendi, M. G. *Nat. Mater.* **2014**, *13*, 796-801.
- (24) Woo, J. Y.; Ko, J.; Song, J. H.; Kim, K.; Choi, H.; Kim, Y.; Lee, D. C.; Jeong, S.; Song, H. J. *Am. Chem. Soc.* **2014**, *136*, 8883-8886.
- (25) Straus, D. B.; Goodwin, E. D.; Gauding, E. A.; Muramoto, S.; Murray, C. B.; Kagan, C. R. *J. Phys. Chem. Lett.* **2015**, *6*, 4605-4609.
- (26) Liu, Y.; Gibbs, M.; Puthussery, J.; Gaik, S.; Ihly, R.; Hillhouse, H. W.; Law, M. *Nano Lett.* **2010**, *10*, 1960-1969.
- (27) Gao, Y.; Talgorn, E.; Aerts, M.; Trinh, M. T.; Schins, J. M.; Houtepen, A. J.; Siebbeles, L. D. A. *Nano Lett.* **2011**, *11*, 5471-5476.
- (28) Gao, Y.; Aerts, M.; Sandeep, C. S. S.; Talgorn, E.; Savenije, T. J.; Kinge, S.; Siebbeles, L. D. A.; Houtepen, A. J. *ACS Nano* **2012**, *6*, 9606-9614.
- (29) Slater, C.; Koster, G. F. *Phys. Rev.* **1954**, *94*, 1498-1524.
- (30) Ashcroft, N. W.; Mermin, N. *Solid State Physics*, Holt Rinehart and Winston, New York, London, 1976.
- (31) Wang, L.-W.; Zunger, A. *Phys. Rev. B* **1996**, *53*, 9579.
- (32) Delerue, C. *Phys. Chem. Chem. Phys.* **2014**, *16*, 25734-25740.
- (33) Sandeep, C. S. S.; ten Cate, S.; Schins, J. M.; Savenije, T. J.; Liu, Y.; Law, M.; Kinge, S.; Houtepen, A. J.; Siebbeles, L. D. A. *Nat. Commun.* **2013**, *4*, 2360, DOI: 10.1038/ncomms3360.

- (34) Sandeep, C. S. S.; Azpiroz, J. M.; Evers, W. H.; Boehme, S. C.; Moreels, I.; Kinge, S.; Siebbeles, L. D. A.; Infante, I.; Houtepen, A. J. *ACS Nano* **2014**, *8*, 11499-11511.
- (35) Giansante, C.; Infante, I.; Fabiano, E.; Grisorio, R.; Suranna, G. P.; Gigli, G. *J. Am. Chem. Soc.* **2015**, *137*, 1875-1886.
- (36) Talapin, D. V.; Murray, C. B. *Science* **2005**, *310*, 86-89.
- (37) Drndic, M.; Jarosz, M. V.; Morgan, N. Y.; Kastner, M. A.; Bawendi, M. G. *J. Appl. Phys.* **2002**, *92*, 7498-7503.
- (38) Talgorn, E.; Abellon, R. D.; Kooyman, P. J.; Piris, J.; Savenije, T. J.; Goossens, A.; Houtepen, A. J.; Siebbeles, L. D. A. *ACS Nano* **2010**, *4*, 1723-1731.
- (39) Quan, Z.; Loc, W. S.; Lin, C.; Luo, Z.; Yang, K.; Wang, Y.; Wang, H.; Wang, Z.; Fang, J. *Nano Lett.* **2012**, *12*, 4409-4413.
- (40) Cho, K.-S.; Talapin, D. V.; W. Gaschler, W.; Murray, C. B. *J. Am. Chem. Soc.* **2005**, *127*, 7140-7147.
- (41) Schliehe, C.; Juarez, B. H.; Pelletier, M.; Jander, S.; Greshnykh, D.; Nagel, M.; Meyer, A.; Foerster, S.; Kornowski, A.; Klinke, C.; Weller, H. *Science* **2010**, *329*, 550-553.
- (42) Evers, W. H.; Goris, B.; Bals, S.; Casavola, M.; de Graaf, J.; van Roij, R.; Dijkstra, M.; and Vanmaekelbergh, D. *Nano Lett.* **2013**, *13*, 2317-2323.
- (43) Treml, B. E.; Robbins, A. B.; Whitham, K.; Smilgies, D.-M.; Thompson, M. O.; and Hanrath, T. *ACS Nano* **2015**, *9*, 4096-4102.
- (44) Evers, W. H.; Schins, J. M.; Aerts, M.; Kulkarni, A.; Capiod, P.; Berthe, M.; Grandidier, B.; Delerue, C.; van der Zant, H. S. J.; van Overbeek, C.; Peters, J. L.; Vanmaekelbergh, D.; Siebbeles, L. D. A. *Nat. Commun.* **2015**, *6*, 8195, DOI: 10.1038/ncomms9195.
- (45) Anderson, P. W. *Phys. Rev.* **1958**, *109*, 1492-1505.

- (46) Guyot-Sionnest, P. *J. Phys. Chem. Lett.* **2012**, *3*, 1169-1175.
- (47) Shabaev, A.; Efros, Al. L.; Efros, A. L. *Nano Lett.* **2013**, *13*, 5454-5461.
- (48) Franceschetti, A.; Fu, H.; Wang, L.-W. & Zunger, A. *Phys. Rev. B* **1999**, *60*, 1819-1829.
- (49) Sills, A.; Harrison, P.; Califano, M. *J. Phys. Chem. Lett.* **2016**, *7*, 31-35.
- (50) An, J. M.; Franceschetti, A.; Dudiy, S.V.; Zunger, A. *Nano Lett.* **2006**, *6*, 2728-2735.
- (51) Goodfellow, B. W.; Yu, Y.; Bosoy, C. A.; Smilgies, D.-M.; Korgel, B. A. *J. Phys. Chem. Lett.* **2015**, *6*, 2406-2412.
- (52) Gómez-Campos, F. M.; Rodríguez-Bolívar, S.; Califano, M. (unpublished)
- (53) Jasieniak, J.; Califano, M.; Watkins, S. E. *ACS Nano* **2011**, *5*, 5888-5902.
- (54) Yu, P.; Cardona, M. *Fundamentals of Semiconductors: Physics and Materials Properties*, 4th edition; Springer, Berlin, Heidelberg, 2010. ISBN 978-3-642-00709-5.
- (55) A larger size distribution leads to a smaller electron mobility, given the position of the factor M - containing the scattering potential - in Eq. (3).